New Phytologist

Research

Methods

X-ray imaging of leaf venation networks

Benjamin Blonder[1,2], Francesco De Carlo[3], Jared Moore[4], Mark Rivers[5] and Brian Enquist[1,2,6]

[1]Department of Ecology and Evolutionary Biology, University of Arizona, 1041 E Lowell St, Tucson, AZ, 85721, USA; [2]Rocky Mountain Biological Laboratory, PO Box 519, Crested Butte, CO, 81224, USA; [3]Argonne National Laboratory, Advanced Photon Source, 9700 South Cass Avenue,Lemont, IL, 60439, USA; [4]Center for Gamma-Ray Imaging, Department of Radiology, University of Arizona, PO Box 245067, Tucson, AZ, 85724, USA; [5]Center for Advanced Radiation Sources, University of Chicago, 9700 South Cass Avenue, Lemont, IL, 60439, USA; [6]Santa Fe Institute, 1399 Hyde Park Road, Santa Fe, NM, 87501, USA

Author for correspondence:
Benjamin Blonder
Tel: +1 520 626 3336
Email: bblonder@email.arizona.edu

Received: *11 June 2012*
Accepted: *27 August 2012*

New Phytologist (2012)
doi: 10.1111/j.1469-8137.2012.04355.x

Key words: imaging, leaf, light source, synchrotron, vein, venation network, X-ray.

Summary

- Leaf venation networks mediate many plant resource fluxes and are therefore of broad interest to research questions in plant physiology, systematics, paleoecology, and physics. However, the study of these networks is limited by slow and destructive imaging methods. X-ray imaging of leaf veins is potentially rapid, of high resolution, and nondestructive.
- Here, we have developed theory for absorption- and phase-contrast X-ray imaging. We then experimentally test these approaches using a synchrotron light source and two commercially available X-ray instruments.
- Using synchrotron light, we found that major veins could be consistently visualized using absorption-contrast imaging with X-ray energies < 10 keV, while both major and minor veins could be consistently visualized with the use of an iodine contrast agent at an X-ray energy of 33.269 keV. Phase-contrast imaging at a range of energies provided high resolution but highlighted individual cell walls more than veins. Both approaches allowed several hundred samples to be processed per d. Commercial X-ray instruments were able to resolve major veins and some minor veins using absorption contrast.
- These results show that both commercial and synchrotron X-ray imaging can be successfully applied to leaf venation networks, facilitating research in multiple fields.

Introduction

Hidden beneath the surface of every leaf is an intricate and beautiful network of veins (Ettingshausen, 1861). This network is built from lignified xylem and phloem tissue and serves multiple functions, including transport of water and sugars, mechanical support, and herbivory resistance (Roth-Nebelsick *et al.*, 2001). Because of this diversity in form and function, these networks are of interest to a wide range of fields. For systematics and evolutionary biology, veins can be useful for taxonomy (Ellis *et al.*, 2009) and for studying climate change and macroevolutionary trends (Boyce *et al.*, 2009; Brodribb & Feild, 2010; Feild *et al.*, 2011). For plant physiologists, veins are key to understanding hydraulics and carbon fluxes (Sack & Holbrook, 2006; Brodribb *et al.*, 2007; Niinemets *et al.*, 2007; Sack *et al.*, 2008; McKown *et al.*, 2010; Blonder *et al.*, 2011). For paleoecology, venation networks may be a useful proxy for climate reconstruction (Manze, 1967; Uhl & Mosbrugger, 1999). For developmental biologists, veins are key to understanding vascular patterning and tissue differentiation (Candela *et al.*, 1999; Scarpella *et al.*, 2010; Sack *et al.*, 2012). For physical scientists, veins provide an insight into the general properties of network formation, resource distribution, and redundancy (Turcotte *et al.*, 1998; Couder *et al.*, 2002; Noblin *et al.*, 2008; Corson, 2010; Katifori *et al.*, 2010; Price *et al.*, 2011b).

Despite broad scientific interest, the study of leaf venation networks has been limited by the difficulty in obtaining high-resolution images. The study of leaf veins is often data-limited (e.g. Price *et al.*, 2011b) because contemporary visualization methods (Ellis *et al.*, 2009; Horn *et al.*, 2009) are slow and destructive, requiring multiple days of incubation and several different chemical treatments. Note that these methods are an advance over historical methods that relied on multi-month degradation of tissues in water (Seba, 1729; Parrish, 1863), or the application of exotic chemicals such as arsenic sulfide (Hill, 1770). Nevertheless, developing faster and less destructive methods to visualize and measure venation networks is a major challenge for the field.

We test the hypothesis that X-ray imaging can greatly increase the speed and reliability of imaging leaf venation networks. X-rays are photons with energies in the range of 10^2–10^6 eV, which is far higher than the 1.7–2.9 eV range of visible light. The light–matter interactions that occur at this energy range are different than for visible light. As a result, there are three useful properties of X-rays for imaging: leaves suffer minimal long-term damage from short exposure to X-rays, enabling reuse of samples for other

© 2012 The Authors
New Phytologist © 2012 New Phytologist Trust

applications; X-rays penetrate deeply, enabling imaging of thick or pubescent leaves without special preparation; high-flux X-ray sources and efficient X-ray detectors enable rapid imaging.

We have developed a theory for phase and absorption-contrast X-ray imaging, and experimentally test this theory on a wide range of leaves prepared with and without an iodine contrast agent. We focused our investigation on X-ray synchrotron light sources (large particle accelerators that generate X-rays through the interaction of relativistic electrons with high magnetic fields). We also assessed the imaging properties of commercially available X-ray systems and compared these methods with extant chemical approaches.

Description

X-ray imaging theory

The interactions of X-rays with matter can be described approximately in terms of the propagation of a plane electromagnetic wave. The amplitude of this wave is proportional to $\mathrm{Re}\left[e^{\frac{2\pi}{\lambda_0}(nz-ct)}\right]$, where Re denotes the real part of a complex number, λ_0 is the vacuum wavelength of the light, c is the vacuum speed of light, z is the thickness of the material, t is the time, and n is the material's refractive index. If we arbitrarily partition n in terms of a real and complex component, $1-\delta-i\beta$, then the previous formula becomes $e^{\frac{2\pi z}{\lambda_0}\beta}\cos\left[\frac{2\pi z}{\lambda_0}(1-ct-\delta)\right]$. Thus, the real component, δ, determines phase shifts, whereas the imaginary component, β, determines absorption. Thus the ratio δ/β measures the relative strength of phase and absorption effects for a material across photon energies, indicating appropriate imaging approaches. Values of δ and β are controlled by the density of the material as well as energy and atomic number-dependent processes such as photoelectric absorption, Compton scattering, and Rayleigh scattering (Seibert & Boone, 2005; Zhou & Brahme, 2008). For the low-atomic-number materials that comprise most biological tissue, β is small and decreases rapidly with increasing photon energy (Hubbell & Seltzer, 2004). However, δ can be high in magnitude and also display wide variability across the X-ray energy range (Fig. 1). For high-atomic-number materials, the value of β can show wide variation as a result of resonant absorption at certain energies. For example, iodine has a Kα-resonance ('K-edge') at 33.169 keV, corresponding to a 2p→1s electronic transition. Low-atomic-number materials have Kα-resonances at much lower energies that are not easily accessed for imaging. Moreover, such low-energy photons have a very low probability of penetrating a thick leaf sample.

Image contrast is achieved by detection of spatial variation in a sample's refractive index, as modulated by the thickness and density of the sample. Two approaches (phase- and absorption-contrast imaging) can be used depending on the X-ray energy and sample properties (Zhou & Brahme, 2008). To understand these two approaches, consider an X-ray source that emits photons that propagate a distance L before interacting with the sample, and that then propagate a further distance d before reaching a detector (Fig. 2). In absorption-contrast imaging, the detector is placed behind the sample. For coherent or monochromatic photon sources (e.g. synchrotron light sources), the geometry is chosen such that that $d \ll L$, which minimizes interference patterns generated from phase-shifted light and maximizes intensity variation as a result of absorbed or transmitted light. For incoherent or polychromatic photon sources (e.g. X-ray tube sources), phase shifts are undetectable and absorption effects necessarily dominate regardless of d or L. Regardless, the intensity I of the image formed at the detector directly reflects spatial variation in total absorption, which is related to the sample's β and thickness τ via the Beer–Lambert law: $I \propto \exp\left[-4\pi\beta\tau/\lambda_0\right]$ (Fig. 3a) (Zhou & Brahme, 2008). Alternatively, in phase-contrast imaging, the detector is placed at a larger distance behind the sample, so that $d < L$. This geometry permits Fresnel diffraction past the sample and generates an interference pattern at the detector (Fig. 3b) that reflects only spatial variation in δ (for the theory, see Cowley, 1995; Snigirev *et al.*, 1995; Weon *et al.*, 2006). For a certain value of d, varied experimentally, the intensity of the interference pattern can result in useful edge enhancement. Thus, by simply varying the sample–detector distance d, an investigator can easily produce both phase- and absorption-contrast images.

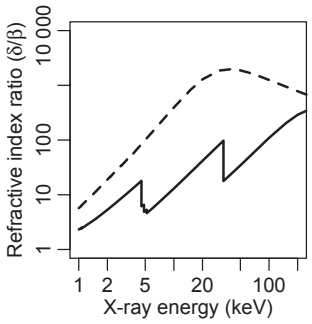

Fig. 1 The relative strength of phase to absorption contrast, δ/β, is determined by a material's complex refractive index, $1-\delta-i\beta$. In soft biological tissue (dashed line), phase contrast dominates absorption contrast at a wide range of X-ray energies. However, the introduction of a heavy element such as iodine (solid line) can increase the relative strength of absorption contrast near atomic resonance energies (e.g. above the iodine Kα edge at 33.169 keV). Data for this figure come from transformed (Zhou & Brahme, 2008) X-ray mass-attenuation coefficients (Hubbell & Seltzer, 2004).

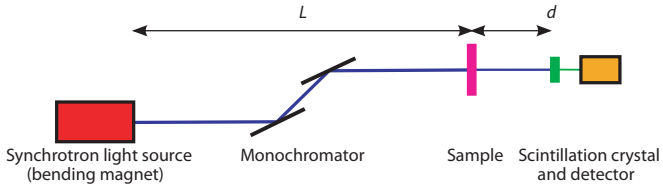

Fig. 2 Geometry for synchrotron X-ray imaging. Collimated X-rays are generated through the interaction of relativistic electrons with a bending magnet. A single X-ray energy is selected via Bragg diffraction by varying the angle of a double crystal monochromator. After propagating a distance L, monochromatic X-rays interact with the sample and then propagate a further distance d before being absorbed by a scintillation crystal and re-emitted as visible photons that are imaged by a detector. For $d \ll L$, absorption-contrast images are obtained, while for some $d < L$, phase-contrast images are obtained. In medical and microfocus X-ray computed tomography (micro-CT) X-ray instruments, the monochromator and scintillation crystal are absent, and X-rays leave the source over a much wider angular range.

© 2012 The Authors
New Phytologist © 2012 New Phytologist Trust

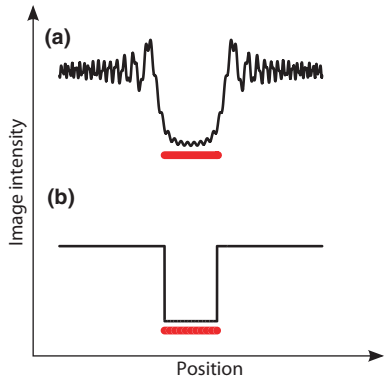

Fig. 3 Contrast mechanisms generate unique spatial distributions of image intensities. Here, predictions are shown for a rectangular object (in red). (a) For phase contrast, Fresnel diffraction over a small object–detector distance yields an intensity distribution that can show edge enhancement. (b) For absorption contrast, X-ray propagation over a minimal object–detector distance yields an intensity distribution corresponding to the outline of the object.

Desirable imaging system properties

The theory described in the previous section provides guidelines for X-ray imaging of leaf venation networks. Because leaves comprise elements with low atomic numbers, absorption contrast should be weak across the X-ray energy range but stronger at low photon energies, with contrast arising from the greater thickness and/or higher density (i.e. β) of veins relative to nonvascular tissue. To improve absorption contrast, leaf veins could be stained with a high-atomic-number contrast agent such as iodine, and imaging could proceed at a photon energy corresponding to an electronic resonance of the contrast agent. Iodine and iodine salts are soluble in water and are commonly used as medical contrast agents (Freudenberger *et al.*, 2001). For monochromatic photon sources, the geometry of the imaging system should also satisfy $d \ll L$. Alternatively, phase contrast should highlight cellular structure in low-atomic-number samples, be strong at a range of photon energies, and not require a contrast agent. In this case, a monochromatic photon source should be used and the geometry of the imaging system should satisfy $d < L$. An ideal X-ray imaging system should meet two additional constraints. Desirable properties include both high brightness (photons second^{-1}, solid angle^{-1}, source area^{-1}, energy bandwidth^{-1}) so that collimated photons reach the sample at a high rate, ensuring fast and low-noise imaging, and also a tunable monochromatic beam, so that photons of a chosen energy can be used to maximize contrast, especially in absorption imaging.

Commercially available X-ray systems have previously been used for imaging plants for artistic (Raikes, 2003) and scientific projects (Pechan & Morgan, 1983; Wing, 1992). Medical diagnostic X-ray instruments are easy to find but are limited by a reliance on X-ray tube sources (which generate a polychromatic beam), film or phosphor detection (which both require a slower development process). More recently, submillimeter-resolution computed tomography (micro-CT) systems are also becoming available at low cost. While these systems do not have monochromatic sources, or $d \ll L$, they do offer digital X-ray detection, high resolution, and a wide range of energy spectra. Tube voltages of *c.* 60 kVp can generate a photon energy spectrum (0–60 keV) that will cover the iodine K-edge. Thus, absorption imaging with iodine contrast may still be possible. These systems have previously been used for a range of biological-imaging applications (Stuppy *et al.*, 2003; Lee & Kim, 2008; Brodersen *et al.*, 2011).

Synchrotron light sources have properties closely matched to an ideal imaging system. They can have much higher brightness (by a factor of up to 10^{10}) than tube sources because of their large size and a variety of relativistic effects (Attwood, 2007). They also can produce photons with a narrow energy bandwidth via the use of crystal monochromators. It is easy to achieve $d \ll L$, because L is typically on the order of 50 m. And finally, rapid imaging is possible using charge coupled device (CCD)/complementary metal oxide semiconductor (CMOS) flat-panel arrays that detect photons emitted by scintillation crystals that absorb X-rays and re-emit them as visible light, or using 'direct detection' flat-panel semiconductor arrays doped with high-atomic-number elements that absorb high-energy photons. Because of these strengths, synchrotron light sources have been used for a range of imaging applications requiring high temporal and spatial resolution for soft-tissue samples (Westneat *et al.*, 2003; Socha *et al.*, 2007; Hwu *et al.*, 2008). The downside of these facilities is their lower accessibility relative to commercially available X-ray systems. Nevertheless, over 70 of these light sources have been built around the world, many of which have beamlines that are suitable for this type of imaging. Beamline sources typically solicit proposals from researchers for experiments to be performed and, once approved, the experiments may be performed at no cost. A list of facilities and a guide to their use is available at http://www.lightsources.org/cms/?pid=1000098 and http://en.wikipedia.org/wiki/List_of_synchrotron_radiation_facilities.

Methods

We made images of leaf venation networks using three different X-ray sources (synchrotron, medical diagnostic, and micro-CT). For the synchrotron, we used the US Department of Energy's Advanced Photon Source (APS) at Argonne National Laboratory (Argonne, IL, USA). For the medical diagnostic X-ray, we used an instrument at the University of Arizona's College of Medicine. For the micro-CT, we used an instrument at the University of Arizona's Radiology Research department. Using these instruments, we varied imaging geometry for absorption and phase contrast. We also tested the effect of the presence/absence of an iodine contrast agent. These experiments are summarized in Table 1.

Synchrotron: absorption- and phase-contrast imaging with no iodine contrast agent

We collected 408 leaves from 44 woody and herbaceous species spanning a wide climate gradient in the Colorado Rocky Mountains. Each of these leaves was pressed flat and dried at 60°C for at least 3 d, after which a 5 × 5 mm^2 section was cut from the lamina of each leaf using a razor blade.

© 2012 The Authors
New Phytologist © 2012 New Phytologist Trust

Table 1 Summary of instruments tested and experiments performed

Experiment		System		
Contrast type	Contrast agent used	Synchrotron light source (3.5 μm resolution)	Medical diagnostic X-ray (50 μm resolution)	Micro-CT X-ray (15 μm resolution)
Absorption	No	Figs S1, S2	Fig. 6	x^1
Absorption	Yes	Fig. 5, Fig. S3	x^2	Fig. 7
Phase	No	Fig. S1	x^3	x^3
Phase	Yes	Fig. S3	x^3	x^3

Some experiments were not possible because of X-ray tube limitations (x^1, low-energy beam not available; x^2, high-energy beam not available; x^3, monochromatic beam not available).

We then imaged these samples at APS's 2-BM beamline during November 2010 in under 2 d. The beamline uses a bending magnet with a double-bounce, multi-layer monochromator to produce high-brightness monochromatic X-rays. Each sample was mounted on small aluminum platform using modeling clay; these platforms were then rapidly transferred by robotic arm to a translation stage placed in the beam path. X-rays were converted to visible light using a lutetium aluminum garnet (LuAG) scintillation crystal and then imaged using a 4× microscope objective and 2048 × 2048 pixel 12-bit CCD array. The system's final resolution was 1.66 μm pixel^{-1}. We fixed L at 55 m while varying d from 0.01 to 0.10 m, and varied the X-ray energy from 7 to 30 keV.

For each sample a bright field (with sample), flat field (no sample), and dark field (no X-rays) were obtained with a maximum exposure time of 450 ms. A final image was calculated as (bright − dark)/(flat − dark) and then local contrast was further enhanced using a contrast-limited adaptive histogram equalization (Zuiderveld, 1994).

Synchrotron: absorption- and phase-contrast imaging with iodine contrast agent

We collected 599 leaves from 37 species and natural hybrids in the silversword alliance spanning a wide climate gradient on the Hawaiian Islands (Carlquist *et al.*, 2003). The analysis of these taxa will be the subject of a forthcoming publication. Each of these leaves was pressed flat and dried at 60°C for at least 2 d. A 5 × 5 mm^2 section was cut from the lamina of each leaf using a razor blade.

We applied iodine contrast agent to each leaf section by transferring the leaf sample to a Petri dish filled with 5 ml of 2% iodine, 4% potassium iodide (w/v) dissolved in water. We covered samples and incubated them at room temperature for 2 d before blotting them dry and pressing them flat in envelopes. To facilitate rapid imaging, we then sandwiched multiple samples in aluminum frames between 13 μm Kapton polyimide films (an X-ray-transparent plastic).

We then imaged these samples at APS's 13-BM-D beamline during October 2011 (Fig. 4) in under 2 d. Monochromatic X-rays were produced using a bending magnet and a double-bounce Si (111) crystal monochromator. We mounted the aluminum frames containing multiple leaf samples to a translation stage placed in the beam path. A LuAG scintillation crystal was used to convert X-rays to visible light photons, which were imaged on to a 1392 × 1040 pixel, 12-bit CCD ray by a 5× magnification microscope objective. The system's final resolution was 3.56 μm pixel^{-1}. We fixed L at 55 m, varied d from 0.01 to 0.20 m, and varied the X-ray energy from 10 to 60 keV.

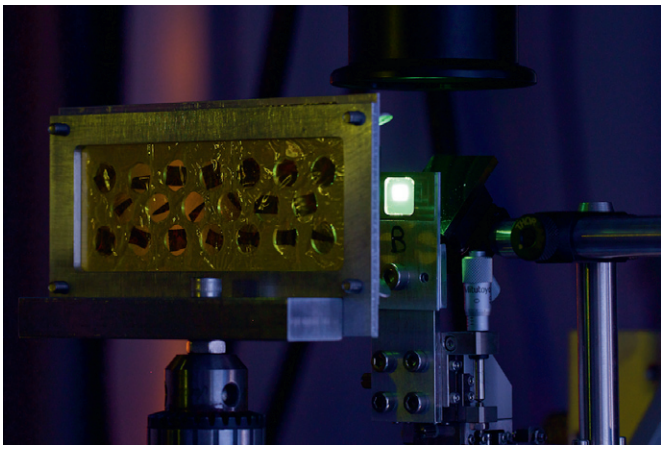

Fig. 4 Leaves being imaged with synchrotron X-rays at beamline 13-BM-D at the Advanced Photon Source. A collimated beam of X-rays incident from the left of the image passes through a leaf sample before being absorbed and re-emitted as green light by a scintillation crystal. This visible light is reflected by a mirror toward a lens and charge coupled device (CCD) camera. In this configuration, 20 leaf samples can be automatically imaged before any human intervention is needed.

For each sample, we obtained 10 bright fields and flat fields with a maximum exposure time of 1700 ms; we then averaged these images to reduce noise. A final image was calculated as (bright average − dark)/(flat average − dark), assuming a constant dark intensity of 100 counts pixel^{-1}. A larger image was then created by stitching images created by repeating the procedure after translating the sample to four different locations. Local contrast was further enhanced using a contrast-limited adaptive histogram equalization (Zuiderveld, 1994).

Medical diagnostic X-ray: absorption-contrast imaging with no iodine contrast agent

We collected leaves from two species grown at the University of Arizona campus arboretum. We immediately placed a leaf in the chamber of a specimen radiography system (Bioptics, Pixarray 100) intended for breast biopsies. The system generates polychromatic X-rays with a 1 mA tube source. Imaging geometry is fixed with

© 2012 The Authors
New Phytologist © 2012 New Phytologist Trust

$L \approx 0.3$ m and $d \approx 0.01$ m. X-rays are detected digitally with a nominal 50 μm pixel^{-1} resolution. For each leaf, we varied tube voltage from 10 to 40 kVp, which yields an X-ray energy spectra peaking between 5 and 20 keV. We chose exposure times that minimized noise (up to 19 s, the longest permitted by integrated dose-restriction software). Images were automatically processed by integrated software, and no further enhancement was performed.

Micro-CT X-ray: absorption-contrast imaging with iodine contrast agent

We prepared leaves with an iodine contrast agent by soaking each in a glass jar filled with 100 ml of 2% iodine, 4% potassium iodide (w/v) dissolved in water. We covered samples and incubated them at room temperature for 2 d before blotting them dry and pressing them flat in envelopes. We immediately placed each leaf in the sample holder of an X-ray computed tomography system (FaCT; Moore, 2011). The system generates polychromatic X-rays using a tungsten-anode, cone-beam-emission X-ray source. The X-ray tube may be operated at a voltage range of 20–130 kVp for currents up to 0.5 mA. The imaging geometry of the system is variable. The source-to-detector distance, $L + d$, is fixed at 270 mm. Geometric magnification (Wing, 1992) is achieved by varying the distance between the source and object, L, between 25 and 245 mm. The magnification factor achieved is given by $(L + d)/L$, such that magnification factor increases by decreasing L. The system uses a 2048 × 1024 pixel, 12-bit silicon CMOS detector coupled to a gadolinium oxide scintillator crystal to detect the incident X-ray photons. With geometric magnification, the effective resolution increases to a maximum of *c.* 15 μm (limited by the effective size of the focal spot of emitted X-rays from the anode). Since the diameter of the focal spot increases linearly with the power at which the tube is operated, we chose a very low operating current of 0.15 mA to maximize resolution. To offset the low photon flux by the small focal spot size, we set the exposure time to 6.7 s, the maximum allowed by the data-acquisition software. Local contrast was further enhanced using a contrast-limited adaptive histogram equalization (Zuiderveld, 1994).

Results

Synchrotron X-ray imaging

Leaf venation imaging without an iodine contrast agent at 2-BM produced images with a wide quality range. Energies above 20 keV resulted in low-contrast images for both phase and absorption contrast. However, at lower energy (8 keV), high-contrast images were obtained (Supporting Information, Fig. S1). It is likely that better images would be obtained at even lower energies, but the design of the beamline's crystal monochromator prevented lower energies from being used. The best absorption-contrast images were obtained at $d = 0.01$ m, the smallest distance permitted by the geometry of the beamline. The best phase-contrast images were obtained at $d = 0.045$ m. While absorption images highlighted major and minor veins, phase images also generated contrast from individual cell walls. Thus, phase contrast was high but not necessarily useful for this application. In general, image contrast for absorption-contrast images was uneven (Fig. S2). Some samples showed clear detail of the leaf's minor venation, whereas others only showed major veins. Veins were also sometimes obscured by trichomes or blurring from multiple layers of cells. Moreover, lateral veins in one *Poa* species were not quite visible.

Imaging with an iodine contrast agent at 13-BM produced consistently high-quality images (Fig. S3). We found that absorption contrast was highest at 33.269 keV (100 eV above the iodine Kα edge) but was also sufficient at lower energies. The best absorption-contrast images were obtained at $d = 0.01$ m, the smallest distance permitted by the geometry of the beamline. The best phase-contrast images were obtained at $d = 0.20$ m. Here, phase-contrast imaging successfully highlighted details of major and minor veins but also highlighted cell walls. Thus, although resolution for phase-contrast imaging was very high, this contrast was also not necessarily useful. Generally, absorption-contrast imaging at the iodine Kα edge provided consistently high-quality images (Fig. 5) for a range of very different species. This result is remarkable given that leaf thicknesses of silversword alliance species can exceed 3000 μm (e.g. *Argyroxiphium sandwicense*, shown in Fig. 5d).

Commercially available X-ray imaging

The medical diagnostic X-ray instrument obtained the best results for leaves with no contrast agent using a tube voltage of 15 kVp, a 1 mA tube current, and a 19.1 s exposure. In both species, major veins were clearly visible but minor veins could not be distinguished (Fig. 6) because of the fundamental resolution limit of the instrument. Because of this limitation we did not pursue this approach further.

The micro-CT instrument obtained the best results for leaves with a contrast agent using a tube voltage of 65 kVp, a tube current of 0.15 mA, and a 6.7 s exposure. In both species investigated, all major and minor veins were clearly visible (Fig. 7). However, the connectivity of the minor venation remained difficult to determine.

Discussion

At the synchrotron facility, we were able to process hundreds of samples d^{-1} with minimal human effort owing to short X-ray exposure times and computer-controlled sample loading. We found that absorption-contrast imaging provided high contrast for major veins in all species and for minor veins in some species at energies of < 10 keV. With the use of an iodine contrast agent, a high contrast for major and minor veins was achieved in all species at 33.269 keV. We also demonstrated that this contrast agent could be easily applied via a simple immersion procedure. Finally, we found that, although phase-contrast imaging provides highly detailed images, it is more suited to imaging of cell wall boundaries than to imaging of venation networks. Phase-contrast imaging may be of more use for thinner botanical samples where details of cellular structure are of interest. However, this entire approach requires that samples and investigators travel to a synchrotron light source, which may be cost-prohibitive for small projects.

© 2012 The Authors
New Phytologist © 2012 New Phytologist Trust

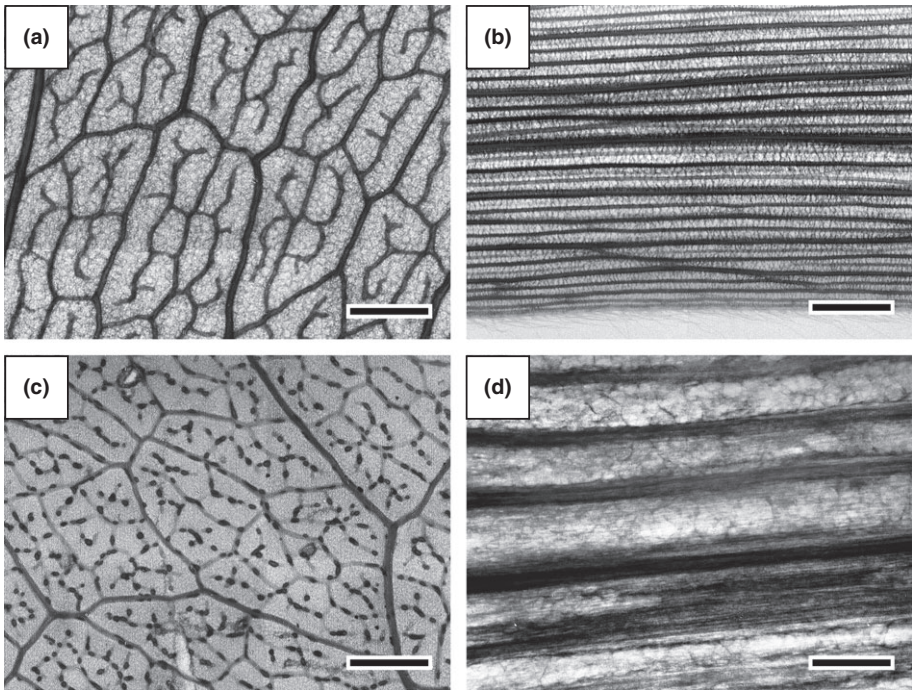

Fig. 5 Example synchrotron images for a range of species imaged with iodine contrast agent using absorption contrast ($d = 0.01$ m) at 33.269 keV. In this configuration, imaging of veins was consistently successful. (a) *Dubautia knudsenii* ssp. *knudsenii* (Asteraceae); (b) *Wilkesia gymnoxiphium* (Asteraceae); (c) *Dubautia latifolia*; (d) *Argyroxiphium sandwicense* ssp. *sandwicense* (Asteraceae). Bars, 1 mm.

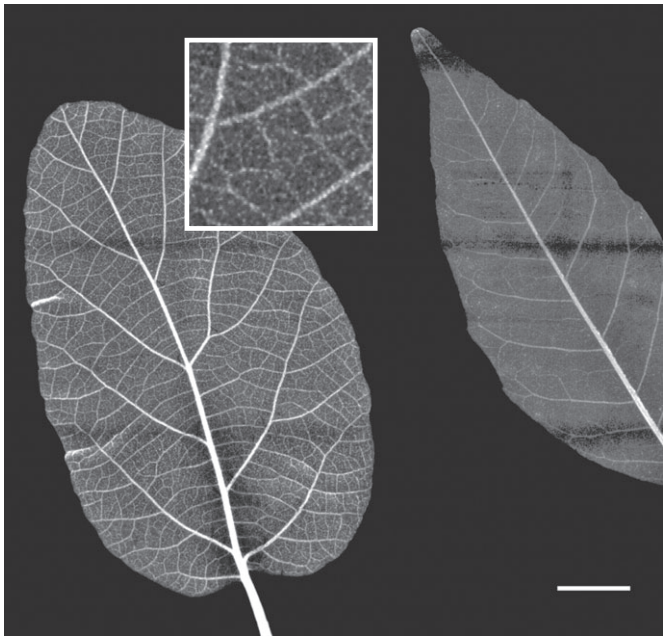

Fig. 6 Example leaf X-rays obtained from a medical diagnostic X-ray instrument. The tube voltage was set to 15 kVp, yielding polychromatic X-rays with peak energies of *c*. 8 keV. For a tube current of 1 mA these images were obtained with a 19.1-s exposure. Bar, 1 cm. The inset box shows maximum detail obtained for the left leaf.

In practice, commercially available X-ray systems could be useful for many biological applications. Most medical diagnostic X-ray instruments operate at low voltage (< 20 kVp) and have sufficient resolution for imaging of major veins with no contrast agent. Because major vein architecture tends to be evolutionarily conserved and useful for taxonomy (Ellis *et al.*, 2009), these instruments could be useful for rapid assay of herbarium samples or field collections in comparative projects. By contrast, micro-CT systems have different practical tradeoffs. Most instruments have X-ray tubes that only operate at high voltages (> 40 kVp), requiring leaves to be treated with a contrast agent before imaging. However, resolution is often much better than in medical diagnostic X-ray systems. Although our micro-CT experiments were unable to resolve the connectivity of the minor venation, this was only because physical constraints in the design of this instrument prevented higher geometric magnification (and resolution) from being reached. Moreover, measurements of minor vein density (which are important for a range of questions; Brodribb *et al.*, 2010) do not require the resolution to measure vein connectivity, so this resolution is likely sufficient for many applications. Other micro-CT instruments should be able to surmount this resolution issue – for example, some industrial nondestructive-test CT systems (e.g. Xradia VersaXRM) can achieve *c*. 900 nm resolution. However, the downsides include a small field of view, because of the limited pixel count of flat-panel detectors, and very long exposure times, because small focal spot sizes require very low tube currents and thus X-ray fluxes. (Phase-contrast imaging is generally not possible in either micro-CT or medical diagnostic X-ray systems, because of nonmonochromatic spectrum of the X-ray source and size limitations on L and d.)

Imaging speeds for synchrotron and commercially available systems are approximately equivalent. Using both types of instruments, we were able to image each sample in < 1 min. This is a notable improvement over the multi-min or multi-h botanical

© 2012 The Authors
New Phytologist © 2012 New Phytologist Trust

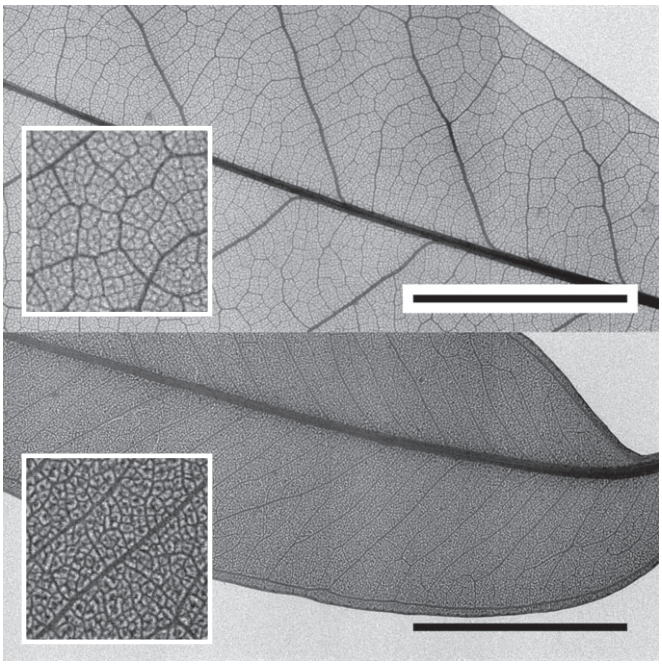

Fig. 7 Example X-ray images obtained for a microfocus X-ray computed tomography systems (micro-CT) instrument. The tube voltage was set to 65 kVp, yielding polychromatic X-rays with peak energies of *c.* 30 keV. For a tube current of 0.15 mA, these images were obtained with a 6 s exposure. Top: *Quercus virginiana*; bottom: *Eucalyptus microtheca*. Bars, 1 cm. The inset boxes show maximum detail obtained for each leaf.

X-rays of previous decades (Wing, 1992) that relied on film instead of digital X-ray detection. Thus, we suggest that micro-CT instruments could be useful for imaging of the minor venation network and its connectivity, enabling more rapid assay of minor vein density and other physiologically important traits for a range of research aims (Brodribb *et al.*, 2010). Future instruments may surmount these practical issues and provide a wider energy range and higher resolution.

We suggest that investigators interested in using X-ray imaging at a medical or micro-CT X-ray instrument can try the imaging system parameters provided here and easily determine if that system will provide sufficient resolution and speed for their application. Our experience is that most instruments built in the last 5 yr will have digital detection systems with adequate resolution, but that older ones (especially phosphor-based systems) will not. The resolution we achieved with micro-CT systems is slightly lower than what is possible using film detection (Wing, 1992), but with the advantage of a much higher speed and no consumable materials.

Synchrotron light sources can address leaf-related research questions that are fundamentally inaccessible to micro-CT or medical diagnostic X-ray systems. Synchrotron imaging can enable real-time study of transport processes in biological networks. For example, studies of vascular development (Scarpella *et al.*, 2010), xylem refilling (Lee & Kim, 2008), long-distance signaling in the phloem (Van Bel, 2003), water re-routing after damage (Katifori *et al.*, 2010), or apoplastic water transport (Canny, 1995) could be achieved via nondestructive X-ray videography using tracers such as iodine or gold nanoparticles. Frame rates of several hundred images s^{-1} can be achieved if a polychromatic beam is used. But some caution should be taken, because the long-term effects of high-X-ray fluxes on living plants are unclear (Simak & Gustafsson, 1953; Sax, 1955; Pechan & Morgan, 1983). Note also that the imaging systems described here are fundamentally limited to a spatial resolution of ~1 μm because of the material properties of scintillation crystals, flat panel detectors, or film (Martin & Koch, 2006). While this resolution is easily sufficient for our application, resolutions of 40 nm (*c.* 10 times better than the diffraction limit for visible light) can be achieved using zone plate optics that directly focus or magnify X-rays (Kirz *et al.*, 1995; Chu *et al.*, 2008).

It is important to note that imaging of leaf venation networks is usually done with the goal of making quantitative measurements of the network (e.g. density of minor veins, or frequency of secondary vein reconnection; Ellis *et al.*, 2009; Blonder *et al.*, 2011; Price *et al.*, 2011b). These statistics can be estimated from images through semi-automatic image-analysis methods (Rolland-Lagan *et al.*, 2009; Price *et al.*, 2011a; Dhondt *et al.*, 2012) or hand-tracing. However, our study's novelty is in the imaging (rather than image analysis) part of this process. We do note that the absorption images made with or without iodine on synchrotron or micro-CT instruments should have sufficient contrast to be useful for this process. As an example (Fig. S4), we show example tracings and measurements of vein density (a commonly measured statistic; Brodribb *et al.*, 2010) for the images presented in Fig. 5.

X-ray imaging compares favorably with existing chemical-preparation methods for visualizing leaf venation networks (Ellis *et al.*, 2009; Blonder *et al.*, 2011). Images of equivalent resolution and contrast can be produced without destructive chemical digestion and slide mounting. Imaging throughput is also much greater. Broadly, our results indicate that commercially available X-ray systems can be used rapidly and nondestructively to make images of leaf venation networks that resolve major veins well and minor veins adequately. Moreover, synchrotron light sources can provide very high-resolution images for detailed imaging of minor veins and likely have great potential for more demanding applications, including cutting-edge questions about xylem and phloem transport. These approaches, coupled with future developments in X-ray imaging technology, should improve research productivity for the study of vascular networks in biology, and a range of applications in plant anatomy, physiology, ecology, and comparative botany.

Acknowledgements

We thank Scott Wing and Owen Atkin for helpful comments during review. Colorado samples were collected with research permits and support from the Rocky Mountain Biological Laboratory (RMBL) and the US Forest Service; and Hawai'i samples with research permits and support from the National Tropical Botanical Garden, Kaua'i State Parks, Hawai'i Department of Land and Natural Resources, Department of Defense Pōhakuloa Training Area, Hawai'i Volcanoes National Park, Haleakalā National Park, The Nature Conservancy, and the US Fish and Wildlife Service. Emma Wollman and Bryan Helm assisted with sample mounting and experimental work at APS.

© 2012 The Authors
New Phytologist © 2012 New Phytologist Trust

Mohsen Haddad-Kaveh provided access to medical X-ray systems. Nathan La Porte and Leah Handel provided logistical support. B.B. was supported by a RMBL summer research fellowship, a Sigma Xi grant in aid of research, and a National Geographic Young Explorers grant. B.J.E. was supported by an NSF ATB award. Work on FaCT was supported by NIBIB grant P41-EB002035. Use of the Advanced Photon Source, an Office of Science User Facility operated for the Department of Energy (DOE) Office of Science by Argonne National Laboratory, was supported by the DOE under contract no. DE-AC02-06CH11357.

References

Attwood DT. 2007 *Soft X-rays and extreme ultraviolet radiation*. Cambridge, UK: Cambridge University Press.

Van Bel AJE. 2003. The phloem, a miracle of ingenuity. *Plant, Cell & Environment* **26**: 125–149.

Blonder B, Violle C, Bentley LP, Enquist BJ. 2011. Venation networks and the origin of the leaf economics spectrum. *Ecology Letters* **14**: 91–100.

Boyce CK, Brodribb TJ, Feild TS, Zwieniecki MA. 2009. Angiosperm leaf vein evolution was physiologically and environmentally transformative. *Proceedings of the Royal Society B: Biological Sciences* **276**: 1771–1776.

Brodersen CR, Lee EF, Choat B, Jansen S, Phillips RJ, Shackel KA, McElrone AJ, Matthews MA. 2011. Automated analysis of three dimensional xylem networks using high resolution computed tomography. *New Phytologist* **191**: 1168–1179.

Brodribb T, Feild T, Jordan G. 2007. Leaf maximum photosynthetic rate and venation are linked by hydraulics. *Plant Physiology* **144**: 1890.

Brodribb TJ, Feild TS. 2010. Leaf hydraulic evolution led a surge in leaf photosynthetic capacity during early angiosperm diversification. *Ecology Letters* **13**: 175–183.

Brodribb TJ, Feild TS, Sack L. 2010. Viewing leaf structure and evolution from a hydraulic perspective. *Functional Plant Biology* **37**: 488–498.

Candela H, Martínez-Laborda A, Micol JL. 1999. Venation pattern formation in *Arabidopsis thaliana* vegetative leaves. *Developmental Biology* **205**: 205–216.

Canny MJ. 1995. Apoplastic water and solute movement: new rules for an old space. *Annual Review of Plant Physiology and Plant Molecular Biology* **46**: 215–236.

Carlquist S, Baldwin BG, Carr GD. 2003 *Tarweeds & silverswords: evolution of the Madiinae (Asteraceae)*. St Louis, MO, USA: Missouri Botanical Garden Press.

Chu YS, Yi JM, Carlo FD, Shen Q, Lee W-K, Wu HJ, Wang CL, Wang JY, Liu CJ, Wang CH, *et al.* 2008. Hard-x-ray microscopy with Fresnel zone plates reaches 40 nm Rayleigh resolution. *Applied Physics Letters* **92**: 103119.

Corson F. 2010. Fluctuations and redundancy in optimal transport networks. *Physical Review Letters* **104**: 048703.

Couder Y, Pauchard L, Allain C, Adda-Bedia M, Douady S. 2002. The leaf venation as formed in a tensorial field. *European Physical Journal B* **28**: 135–138.

Cowley J. 1995. *Diffraction physics*. Amsterdam, the Netherlands: Elsevier.

Dhondt S, Van Haerenborgh D, Van Cauwenbergh C, Merks R, Philips W, Beemster G, Inzé D. 2012. Quantitative analysis of venation patterns of Arabidopsis leaves by supervised image analysis. *The Plant Journal* **69**: 553–563.

Ellis B, Daly DC, Hickey LJ, Mitchell J, Johnson K, Wilf P, Wing S. 2009 *Manual of leaf architecture*. New York, NY, USA: New York Botanical Garden.

Ettingshausen CV. 1861. *Die Blatt-Skelette der Dikotyledonen, mit besonderer Ru cksicht auf die Untersuchung und Bestimmung der fossilen Pflanzenreste*. Wien, Germany: Kais. Ko n. Hof- und Staatsdr.

Feild TS, Brodribb TJ, Iglesias A, Chatelet DS, Baresch A, Upchurch GR Jr, Gomez B, Mohr BAR, Coiffard C, Kvacek J, *et al.* 2011. Fossil evidence for Cretaceous escalation in angiosperm leaf vein evolution. *Proceedings of the National Academy of Sciences, USA* **108**: 8363–8366.

Freudenberger J, Hell E, Knüpfer W. 2001. Perspectives of medical x-ray imaging. *Nuclear Instruments & Methods in Physics Research Section A* **466**: 99–104.

Hill J. 1770. *The construction of timber*. London, UK.

Horn JW, Fisher JB, Tomlinson PB, Lewis CE, Laubengayer K. 2009. Evolution of lamina anatomy in the palm family (Arecaceae). *American Journal of Botany* **96**: 1462–1486.

Hubbell JH, Seltzer SM. 2004. *Tables of X-ray mass attenuation coefficients and mass energy-absorption coefficients (version 1.4)*. Gaithersburg, MD, USA: National Institute of Standards and Technology.

Hwu Y, Tsai WL, Chang HM, Yeh HI, Hsu PC, Yang YC, Su YT, Tsai HL, Chow GM, Ho PC, *et al.* 2008. Imaging cells and tissues with refractive index radiology. *Biophysical Journal* **87**: 4180–4187.

Katifori E, Szöllősi GJ, Magnasco MO. 2010. Damage and fluctuations induce loops in optimal transport networks. *Physical Review Letters* **104**: 048704.

Kirz J, Jacobsen C, Howells M. 1995. Soft x-ray microscopes and their biological applications. *Quarterly Reviews of Biophysics* **28**: 33–130.

Lee S-J, Kim Y. 2008. *In vivo* visualization of the water-refilling process in xylem vessels using X-ray micro-imaging. *Annals of Botany* **101**: 595–602.

Manze U. 1967 *Die Nervaturdichte der Blätter als Hilfsmittel der Paläoklimatologie*, Thesis. Universität zu Köln, Germany.

Martin T, Koch A. 2006. Recent developments in X-ray imaging with micrometer spatial resolution. *Journal of Synchrotron Radiation* **13**: 180–194.

McKown AD, Cochard H, Sack L. 2010. Decoding leaf hydraulics with a spatially explicit model: principles of venation architecture and implications for its evolution. *The American Naturalist* **175**: 447–460.

Moore JW. 2011 *Adaptive X-ray computed tomography*. Tucson, AZ, USA: The University of Arizona.

Niinemets U, Portsmuth A, Tobias M. 2007. Leaf shape and venation pattern alter the support investments within leaf lamina in temperate species: a neglected source of leaf physiological differentiation? *Functional Ecology* **21**: 28–40.

Noblin X, Mahadevan L, Coomaraswamy IA, Weitz DA, Holbrook NM, Zwieniecki MA. 2008. Optimal vein density in artificial and real leaves. *Proceedings of the National Academy of Sciences, USA* **105**: 9140–9144.

Parrish E. 1863 *The phantom bouquet: a popular treatise on the art of skeletonizing leaves and seed-vessels and adapting them to embellish the home of taste*. Philadelphia, PA, USA: JB Lippincott.

Pechan PM, Morgan DG. 1983. The use of radiography in studies of plant development *in vivo*. *Planta* **159**: 476–481.

Price C, Symonova O, Mileyko Y, Hilley T, Weitz J. 2011a. Leaf extraction and analysis framework graphical user interface: segmenting and analyzing the structure of leaf veins and areoles. *Plant Physiology* **155**: 236–245.

Price C, Wing S, Weitz JS. 2011b. Scaling and structure of dicotyledonous leaf venation networks. *Ecology Letters* **15**: 87–95.

Raikes M. 2003. Floral radiography: using x rays to create fine art. *Radiographics* **23**: 1149–1154.

Rolland-Lagan A-G, Amin M, Pakulska M. 2009. Quantifying leaf venation patterns: two-dimensional maps. *The Plant Journal* **57**: 195–205.

Roth-Nebelsick A, Uhl D, Mosbrugger V, Kerp H. 2001. Evolution and function of leaf venation architecture: a review. *Annals of Botany* **87**: 553–566.

Sack L, Dietrich EM, Streeter CM, Sanchez-Gomez D, Holbrook NM. 2008. Leaf palmate venation and vascular redundancy confer tolerance of hydraulic disruption. *Proceedings of the National Academy of Sciences, USA* **105**: 1567–1572.

Sack L, Holbrook NM. 2006. Leaf hydraulics. *Annual Review of Plant Biology* **57**: 361–381.

Sack L, Scoffoni C, McKown AD, Frole K, Rawls M, Havran JC, Tran H, Tran T. 2012. Developmentally based scaling of leaf venation architecture explains global ecological patterns. *Nature Communications* **3**: 837.

Sax K. 1955. The effect of ionizing radiation on plant growth. *American Journal of Botany* **42**: 360–364.

Scarpella E, Barkoulas M, Tsiantis M. 2010. Control of leaf and vein development by auxin. *Cold Spring Harbor Perspectives in Biology* **2**: a001511.

Seba A. 1729. The anatomical preparation of vegetables. *Philosophical Transactions* **36**: 441–444.

Seibert J, Boone J. 2005. X-ray imaging physics for nuclear medicine technologists. Part 2: x-ray interactions and image formation. *Journal of Nuclear Medicine Technology* **33**: 3–18.

Simak M, Gustafsson Å. 1953. X-ray photography and sensitivity in forest tree species. *Hereditas* **39**: 458–468.

© 2012 The Authors
New Phytologist © 2012 New Phytologist Trust

Snigirev A, Snigireva I, Kohn V, Kuznetsov S, Schelokov I. 1995. On the possibilities of x-ray phase contrast microimaging by coherent high-energy synchrotron radiation. *Review of Scientific Instruments* **66**: 5486–5492.

Socha JJ, Westneat MW, Harrison JF, Waters JS, Lee W-K. 2007. Real-time phase-contrast x-ray imaging: a new technique for the study of animal form and function. *BMC Biology* **5**: 6.

Stuppy W, Maisano J, Colbert M, Rudall P, Rowe T. 2003. Three-dimensional analysis of plant structure using high-resolution x-ray computed tomography. *Trends in Plant Science* **8**: 2–6.

Turcotte DL, Pelletier JD, Newman WI. 1998. Networks with side branching in biology. *Journal of Theoretical Biology* **193**: 577–592.

Uhl D, Mosbrugger V. 1999. Leaf venation density as a climate and environmental proxy: a critical review and new data. *Palaeogeography, Palaeoclimatology, Palaeoecology* **149**: 15–26.

Weon B, Je J, Hwu Y, Margaritondo G. 2006. Phase contrast X-ray imaging. *International Journal of Nanotechnology* **3**: 280–297.

Westneat M, Betz O, Blob R, Fezzaa K, Cooper W, Lee W. 2003. Tracheal respiration in insects visualized with synchrotron x-ray imaging. *Science* **299**: 558–560.

Wing S. 1992. High-resolution leaf x-radiography in systematics and paleobotany. *American Journal of Botany* **79**: 1320–1324.

Zhou S-A, Brahme A. 2008. Development of phase-contrast X-ray imaging techniques and potential medical applications. *Physica Medica* **24**: 129–148.

Zuiderveld K. 1994. Contrast limited adaptive histogram equalization. In: Heckbert P ed. *Graphic Gems IV*. San Diego, CA, USA: Academic Press Professional, 474–485.

Supporting Information

Additional Supporting Information may be found in the online version of this article.

Fig. S1 Comparison of phase and absorption contrast from a leaf without iodine contrast agent.

Fig. S2 Example synchrotron images for a range of species imaged without iodine contrast agent using absorption contrast.

Fig. S3 Representative synchrotron images from leaves with iodine contrast agent.

Fig. S4 Vein measurements for the images shown in Fig. 5.

Please note: Wiley-Blackwell are not responsible for the content or functionality of any supporting information supplied by the authors. Any queries (other than missing material) should be directed to the *New Phytologist* Central Office.

© 2012 The Authors
New Phytologist © 2012 New Phytologist Trust